Journal of Neuroscience Methods 263 (2016) 95–102

Contents lists available at ScienceDirect

Journal of Neuroscience Methods

journal homepage: www.elsevier.com/locate/jneumeth

Basic neuroscience

Verification of multichannel electrode array integrity by use of cross-channel correlations

Nicholas V. Swindale*, Martin A. Spacek

Department of Ophthalmology and Visual Sciences, University of British Columbia, Eye Care Centre, 2550 Willow St., Vancouver, BC, Canada V5Z 3N9

HIGHLIGHTS

- Use of multi-channel electrode arrays (MEAs) for extracellular recording requires knowledge of the location and functional status of each channel.
- Experience with recordings from our own and other laboratories suggests that shorted and mislocalised channels are often undetected.
- Measurements of channel impedances prior to recording do not always identify problems, or those that arise after testing.
- Our method presents to the user, immediately prior to spike-sorting, with a list of potentially problematic channels.
- Correction of these errors by masking or re-labelling channels can improve subsequent spike sorting.

ARTICLE INFO

Article history:
Received 1 December 2015
Received in revised form 19 January 2016
Accepted 4 February 2016
Available online 11 February 2016

Keywords:
Multi-electrode arrays
Extracellular potentials
Spike-sorting

ABSTRACT

Background: The use of multichannel electrode arrays (MEAs) presents a number of practical challenges to experimenters including correctly labelling different recording channel locations and identifying sites that may be non-functional or short-circuited. These challenges are likely to increase as the number of sites used in recording increases.
New method: This paper presents a simple method for assessing MEA integrity based on the observation that physiologically induced signal correlations between nearby channels fall off with distance. Channels that violate this relationship are flagged as being potentially problematic.
Results: The method is able to present to the user a list of potentially faulty channels for further inspection. Underlying problems include non-functional, shorted and mislocalised channels and channels carrying spurious noisy signals unrelated to those on other channels.
Comparison with existing methods: Computational methods which automatically screen MEAs for faulty electrode channels do not appear to exist in the literature. Currently a user would have to examine single channels, or channel pairs, individually, which would be very time-consuming.
Conclusions: Shorted or mislocalised channels may be more prevalent in MEA recordings than users suspect. The paper presents a simple screening method for identifying such channels prior to carrying out spike-sorting.

1. Introduction

Multichannel electrode arrays (MEAs) are increasingly being used to make electrophysiological recording from different brain regions (Drake et al., 1988; Buzsáki, 2004; Blanche et al., 2005; Berényi et al., 2014). As with tetrodes, sites are typically placed sufficiently close together (*e.g.* 25–70 μm) that the signals from a single neuron will be detected on several adjacent sites. Taking the shape of the spike waveform across several sites into account can significantly improve subsequent sorting of spikes (Gray et al., 1995; Harris et al., 2000; Blanche et al., 2005; Swindale and Spacek, 2014; Kadir et al., 2014; Rossant et al., 2015). This requires that the user knows the spatial position of each site and also requires identification of sites that may be non-functional or short-circuited because of manufacturing defects. Non-functional channels can be identified on the basis of prior impedance testing, with exceptionally low or high values indicating channels that may be shorted or open-circuit respectively. However these tests do not always yield unambiguous results and it may be hard to predict the functional status of a channel based on them. The demands in assessing electrode integrity are likely to become unusually high for electrodes with large numbers of sites (*e.g.*>64) where

* Corresponding author. Tel.: +1 604 875 5379; fax: +1 604 875 4663.
E-mail address: swindale@mail.ubc.ca (N.V. Swindale).

http://dx.doi.org/10.1016/j.jneumeth.2016.02.009
0165-0270/

manual inspection and maintenance of records may be tedious. In this paper we present a simple method for verifying MEA integrity that can be applied to recordings as a screening test immediately before embarking on spike sorting. The method makes use of the observation that, in the brain, electrical signals in the spike-frequency range (>500 Hz) have correlations that fall off roughly exponentially on a scale of 50–200 μm, which is comparable to that of the site spacing on most electrodes. A plot showing the signal correlation for every pair of sites as a function of distance is constructed and a smooth function approximating the decline in correlation with distance is calculated. Points that deviate significantly from the curve indicate different possible problems based on the type of deviation. For example, channel-pair correlations that are consistently close to zero for a particular channel indicate that it is probably non-functional. Correlations close to 1 indicate that the pair is likely short-circuited. Points that differ in other ways from the average may indicate channels that have been wrongly labelled and hence mislocalised. We demonstrate how the method works in recordings made with a variety of MEA designs in different species and brain areas.

2. Methods

Procedures were initially tested on recordings made with 54-channel polytrodes (NeuroNexus) in anesthetized cat visual cortex using methods described in detail elsewhere (Blanche et al., 2005; Swindale and Spacek, 2014). Additional tests were done on MEA recordings made in different laboratories, including recordings from anesthetized cat lateral geniculate nucleus (LGN), primate V4, rat entorhinal cortex and rat hippocampal area CA1. Table 1 gives details of all the datasets that were used in the study. The recordings in datasets R1 and R2 had been band pass filtered in hardware from 0.5 to 6 kHz before being digitized with 12 bit resolution. The recordings in datasets R3–R6 had been digitized at 16-bit resolution with no pre-filtering. For these recordings a high-pass 4 pole Butterworth filter with $f_0 = 0.5$ kHz was applied to remove local field potential signals that would otherwise induce large positive correlations between channels. Pearson's correlation values were calculated for 100,000 randomly selected points in the recording. This set of points was used to calculate the correlation, $c_{n,m}$, for every channel pair (n, m), $n \neq m$, where $1 \leq n, m \leq N$, and N is the total number of channels on the electrode. For an electrode with N channels, this results in $N(N-1)/2$ values. Note that because Pearson's correlation is a normalised value, it is insensitive to gain variations that might be present across channels. These values were then graphed as a function of the distance, x, between the channel pair. A smooth function

$$C(x) = \frac{1 + C_0 a x^{\beta}}{1 + a x^{\beta}} \tag{1}$$

was used to model the dependence of the correlation on channel separation distance x. By design this has the value $C = 1$ at $x = 0$ and $C \rightarrow$ a baseline, C_0, as $x \rightarrow \infty$. Parameters C_0, a and the exponent β. were adjusted using Levenburg–Marquardt optimization (Press et al., 1994) to minimize the sum-of-squares error. This function fit the data well, though we know of no empirical justification for it.

The extent to which individual channels conformed to the relationship obtained with the resulting smooth curve was measured by calculating the average signed deviation, e_n of the set of points belonging to channel n, from the fitted function, *i.e.*

$$e_n = \frac{1}{N} \sum_{m=1, m \neq n}^{N} \left[c_{n,m} - C(x_{n,m}) \right]. \tag{2}$$

In addition, the r.m.s. value, d_n, of the deviations was calculated, *i.e.*

$$d_n = \left\{ \frac{1}{N} \sum_{m=1, m \neq n}^{N} \left[c_{n,m} - C(x_{n,m}) \right]^2 \right\}^{1/2} \tag{3}$$

values of e_n and d_n were then each separately normalised by subtracting the mean and dividing by the standard deviation, taken over all the channels, to give values $\bar{e}_n$ and $\bar{d}_n$, respectively. These values can then be interpreted in terms of standard deviation units, *i.e.* z-scores. Plots of $\bar{e}_n$ *vs* $\bar{d}_n$ are referred to as deviation plots in what follows. Although the absolute value of $\bar{e}_n$ is often correlated with $\bar{d}_n$ the two measures give different kinds of information about deviating channels. Large negative values of $\bar{e}_n$ are likely to indicate non-functioning channels, owing to consistently lower than average correlation values with nearby channels. Large positive values of $\bar{d}_n$ are more likely to indicate mislocalised channels since correlation values may equally well be above or below the fitted function if x-values are incorrect. The use of two slightly different measures of deviation also has the advantage of allowing channel numbers (not shown here for reasons of clarity) to be shown on 2-dimensional plots, allowing outlying channels to be immediately identified by number. Alternatively, or in addition, lists of channels sorted by deviation can be produced and displayed as a table of possible problems. In the tests shown here, values of signed deviation $\bar{e}_n < -2.5$ were used to identify channels that were likely to be non-functional and values of $\bar{d}_n > 2.5$ were used to identify putatively mislocalised channels. These thresholds are shown as dashed lines in Figs. 1–3. The choice of a threshold of 2.5 is somewhat arbitrary: if scores are normally distributed, values >2.5 or <−2.5 would have a 0.6% chance of occurring. Channel pairs (n, m) were identified as being possibly shorted if their correlation, $c_{n,m} > 0.8$. Such pairs typically had values of $\bar{d}_n > 2.5$ though not always. Large values of C_0, indicated the presence of common noise in the recording (or residual field potential signals or other biophysical signals with a broad spatial distribution); their presence or absence had little impact on the deviation measures.

The procedures described in this paper are incorporated into the spikesorting program 'SpikeSorter' which is freely available on request.

3. Results

Fig. 1A shows an example of a correlation-distance graph obtained from all 54 channels of a 2 column polytrode (dataset R1, Table 1). Two channels of this electrode had been grounded prior to the recording on the basis of impedance tests, although signals from the grounded channels were recorded. The correlation graph shows many channel pairs deviating from the majority with correlation values close to zero. The graph does not allow identification of the specific channels giving rise to the aberrant values, however the corresponding deviation plot (Fig. 1B), where single points correspond to particular channels, shows two deviating channels which together would contribute 53 + 52 = 105 points, shown in red in Fig. 1A. These channels were the ones that had been grounded and when they were masked, and the deviation values recomputed, obvious outliers were no longer present in the correlation-distance function (Fig. 1C) or the deviation plot (Fig. 1D).

Fig. 2A shows a similar example of a correlation-distance function obtained from all 54 channels of a 3 column polytrode (dataset R2, Table 1). The graph shows a variety of outlying points, some with relatively high channel pair correlation values and some values close to zero. The deviation plot (Fig. 2B) identified 3 outlying channels. Two of these had previously been grounded on the basis of abnormally high impedance values (2 channels > 10 MΩ) and

Table 1
Summary of datasets. Datasets R1, R2 are from the authors' laboratory; additional recordings were kindly supplied by C. Baker (R3) and Y. Xiao and A. Khachatryan (R4). Datasets R5 and R6 are from recording ec014.716 downloaded from the CRCNS datasharing website (https://crcns.org/). This recording was made with electrodes simultaneously in regions CA1 and entorhinal cortex, by K. Mizuseki and G. Buzsaki. It was split into two for the purposes of comparing the two areas. Channel spacing gives the range of nearest neighbour distances.

Recording	Species	Region	Channels	Layout	Channel spacing (μm)	Duration (mins)
R1	Cat	Area 17	54	2 Columns, hexagonal	50	4
R2	Cat	Area 17	54	3 Columns, hexagonal	64	8
R3	Cat	LGN	32	Single row	50	42
R4	Macaque	V4	64	8 × 8 'Buzsaki'	21–33	28
R5	Rat	CA1	64	8 × 8 'Buzsaki'	21–40	20
R6	Rat	Entorhinal	32	4 × 8 'Buzsaki'	21–40	20

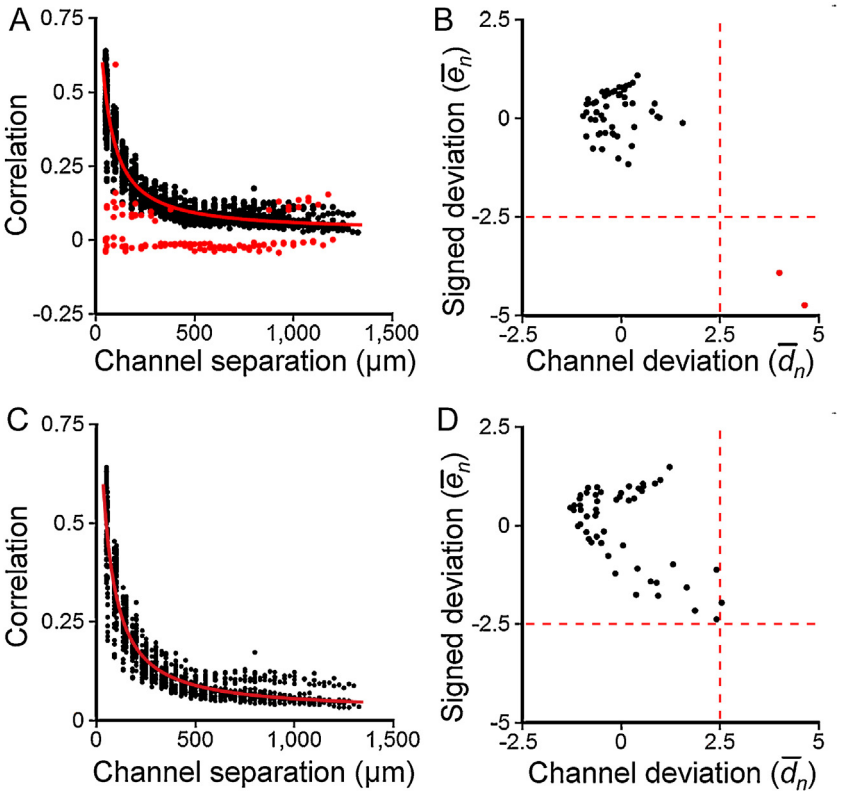

Fig. 1. Channel correlation diagrams for a 54 channel (2-column) electrode (dataset R1, Table 1). (A) Channel pair correlation as a function of distance for all channels (1431 pairs) together with the fitted function (Eq. (1)). In this, and subsequent figures, channel pairs where one (or both) channels have abnormal values of $\bar{e}_n$ or $\bar{d}_n$ are shown in red. (B) Shows, for each channel, the net signed deviation ($\bar{e}_n$, vertical axis) *vs.* the r.m.s. deviation ($\bar{d}_n$, horizontal axis) in normalised (z-score) units. Dashed lines in this, and subsequent figures, show the thresholds of −2.5 and 2.5 that were applied to the values of $\bar{e}_n$ and $\bar{d}_n$, respectively. Note the two outlying points (coloured red) with large negative signed deviations. (C) Shows the channel correlation diagram with these two outlying channels masked and (D) shows the corresponding deviation plot (For interpretation of the references to color in this figure legend, the reader is referred to the web version of this article.).

the third grounded because of an abnormally low value (0.05 MΩ). When these 3 channels were masked, the correlation-distance plot (Fig. 2C) showed only a single outlying channel pair with a relatively high correlation of $c = 0.873$. This pair of channels had impedances of roughly half those of other channels on the probe (0.56 MΩ *vs* a mean of 1.3 MΩ). Although this channel pair was an outlier on the correlation plot, the corresponding deviation plot (Figure 2D) showed no anomalies.

MEA recording data from other laboratories, obtained with a variety of electrode designs in different brain regions (Table 1) was also examined (Fig. 3). As in datasets R1 & R2, all of these recordings showed correlation values around 0.3–0.7 for the smallest channel separations, together with a decline to baseline values at larger separations. The falloff with distance was more rapid, and the baseline correlation lower, in data from primate V4 (Fig. 3B) and less rapid in cat LGN (Fig. 3A), rat CA1 (Fig. 3C) and entorhinal cortex (Fig. 3D). In dataset R4 (Fig. 3B) two pairs of points had correlation values of 0.999 and 0.996, presumably as a result of shorted channels. The deviation values (shown in red in Fig. 3B) of the corresponding 4 channels ranged from 2.96 to 4.19. Raw voltage traces for a subset of channels from this dataset, including two of the channels identified as shorted (channels 42 and 52) are shown in Fig. 4A. In dataset R5 (Fig. 3C) two outlying points with high correlation values ($c = 0.905$ and 0.931) were also identified with deviation values ranging from 2.95 to 3.52. Raw voltage traces including the outlying channel pairs (channels 17, 19, 21 and 23) are shown in Fig. 4B. No abnormalities were identified in datasets R3 or R6 (Fig. 3A and D).

Grounded channels are identified in these tests not because their signals are of lower amplitude (the correlation values are insensitive to differences in channel gains) but because their signals are less well correlated with the signals on other channels than would be expected based on the majority of cross-channel correlations. Hence the tests ought to be able to identify channels carrying spurious signals, not necessarily signals of low amplitude. We tested this by adding Gaussian noise to a single channel, with a standard deviation that was a fixed multiple, M, of the standard

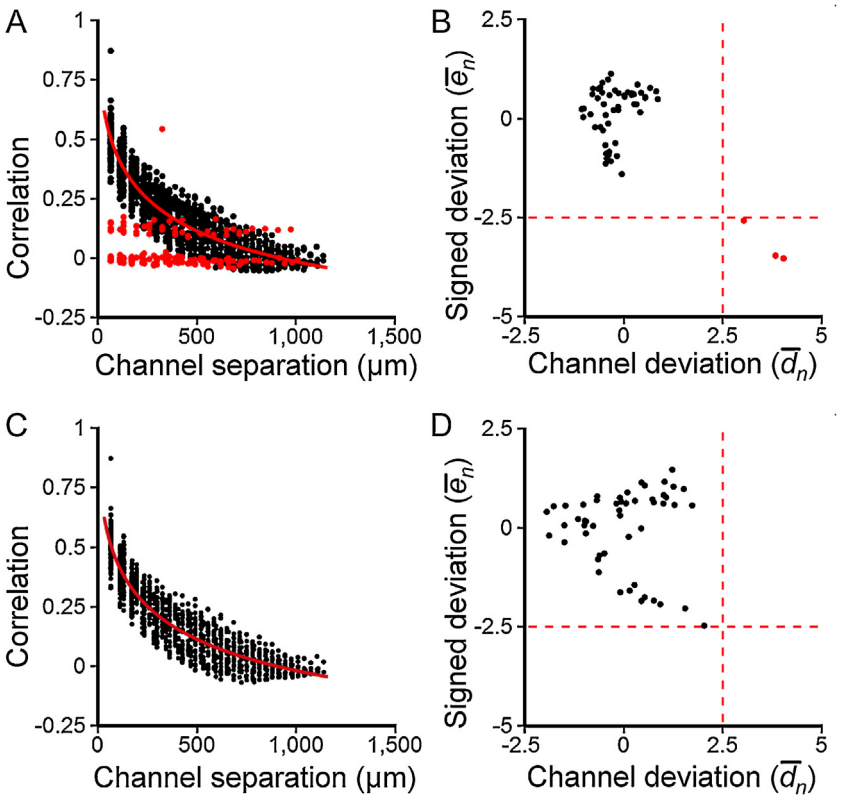

Fig. 2. Channel correlation diagrams for a 54 channel (3-column) electrode (dataset R2, Table 1). (A) Channel pair correlations as a function of distance for all 54 channels together with the fitted function (Eq. (1)). (B) A graph of signed deviation (vertical axis) *vs.* the r.m.s. deviation (horizontal axis) for all 54 channels, showing three outlying points (red). (C) Shows the channel correlation diagram with these channels masked and D shows the corresponding deviation plot (For interpretation of the references to color in this figure legend, the reader is referred to the web version of this article.).

deviation, σ_n of the voltage values on the channel, and then calculating the value of the signed deviation, $\bar{e}_n$ for the channel. The results (Fig. 5) showed that, in all six datasets, noise of >2.0σ_n caused the value of $\bar{e}_n$ to fall below the detection threshold of −2.5. Detection was most sensitive in datasets R3, R5 & R6 where correlations fell off more gradually than in other recordings, and least sensitive in set R2, where correlation values seemed more scattered overall, and in set R4, where correlations fell off rapidly with distance.

We tested the ability of the method to detect mislocalised (or mislabelled) channels by swapping the spatial locations of a single pair of channels and recalculating the deviation values for the recording. This test was done after masking any non-functional or shorted channels, identified as described above. A swapped channel was considered to have been correctly identified if $\bar{d}_n \geq 2.5$. In the absence of swaps this yielded a false positive rate of 1.33% (4 out of 300 channels). Swaps were performed for all channel pairs and the percentage of correct identifications was graphed as a function of distance between channels (Fig. 6). These results show that mislocalised channels will nearly always be identified by this method, provided they are greater than 200 μm apart.

Recordings made with the 3-column electrode used for recording R2 placed in a beaker of saline (Fig. 7) showed a markedly dichotomous pattern of correlations with little or no distance dependence. Inspection of electrode layout diagrams showed that channel pairs that fell into the set with higher correlations were grouped into consecutively numbered sets of 16 (*i.e.* channels 1–16, 17–32, 33–48 and 49–54). Thus correlations between pairs within each set were in the high group, and correlations between pairs in different sets were in the low group. This suggested channel crosstalk originating somewhere in the hardware between the electrode and computer though we were unable to determine the exact origin. Some indications of a related non-uniform distribution of correlations were visible in the *in vivo* recording from the same electrode (Fig. 2C) and also in the recordings from a different electrode (Fig. 1C, points separated by >500 μm). The dichotomy is presumably less evident in the physiological recording than in the saline ones because the physiological correlations outweigh, or swamp those due to crosstalk. The deviation plots for this recording also identified the same set of outliers that was identified in the physiological recordings made with the electrode (Fig. 2C).

Given the lack of any obvious effect of channel separation in the saline recordings it seems reasonable to conclude that the increase in correlation with decreasing channel separation seen in the *in vivo* recordings has a biological origin. Although large amplitude spikes with signals spreading across spatially adjacent channels might seem the most likely source of this we considered it unlikely for two reasons. First, spikes are relatively sparsely occurring events and the majority of randomly chosen points contributing to the correlation most likely came from sections of recording where obviously detectable spikes were absent. Secondly, we did tests where we detected spikes using a relatively unselective low-amplitude bipolar detection threshold of 50 μV, and then masked out regions of recording, on all the channels, that fell within ±0.5 ms of the detection time. The correlation-distance plots from such spike-masked recordings showed a similar distance dependence to those obtained without masking (Fig. 8) albeit with a slightly faster decay with distance than when spike signals were present (compare dashed *vs.* continuous lines on the Figure) for 5 out of the 6 recordings. It is possible that large numbers of unresolvable low-amplitude spikes are the source of the correlation but this remains to be demonstrated.

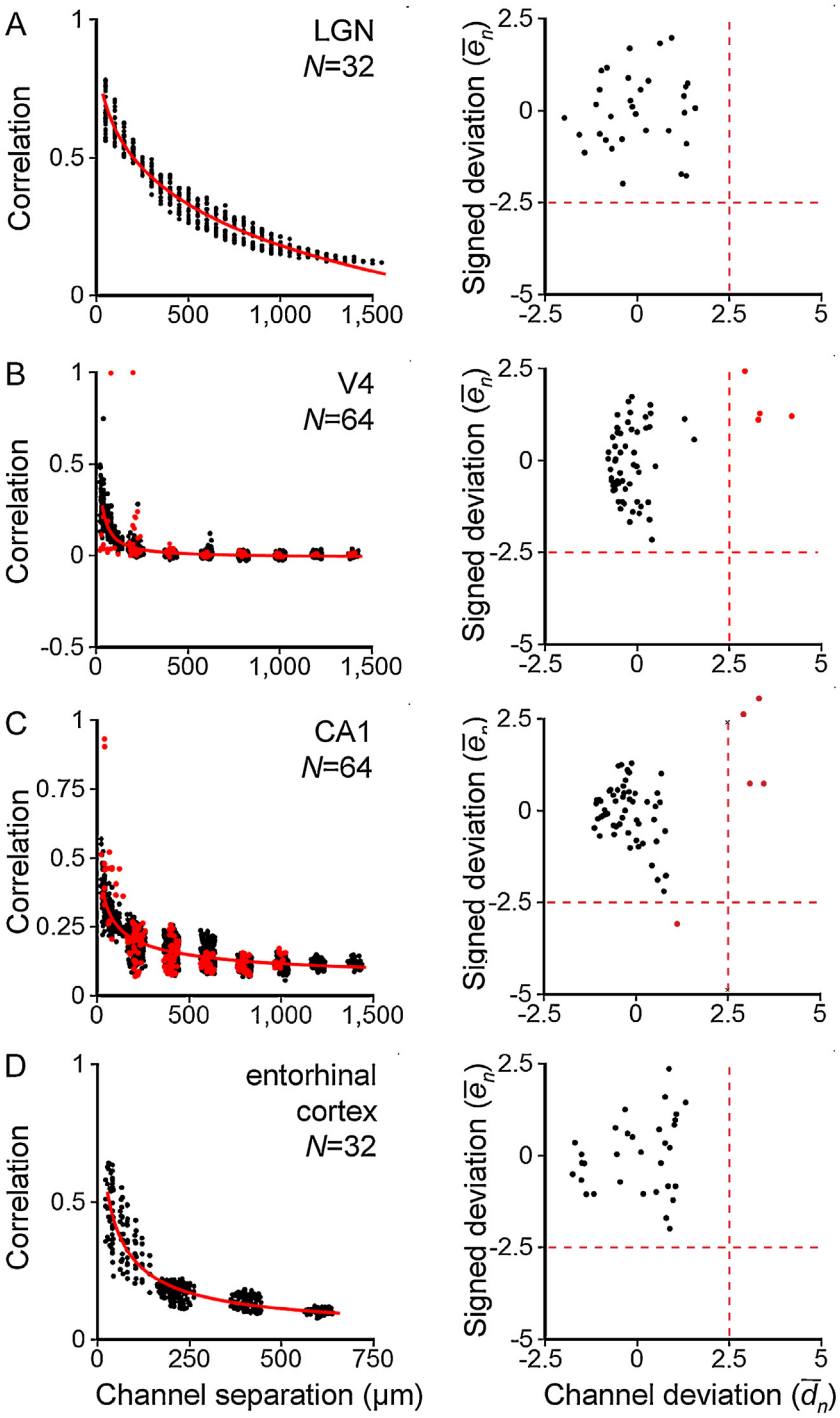

Fig. 3. Additional correlation-distance (left hand panels) and deviation (right hand panels) plots for different electrode types and brain regions (datasets R3–R6, Table 1). *N* gives the number of channels for each electrode type. (A) From a 32 channel linear array in cat LGN; (B) from a 64 channel array in macaque V4; (C) from a 64 channel array in rat CA1; (D) from a 32 channel array in rat entorhinal cortex.

4. Discussion

Knowing the correct spatial location of MEA channels, and which are functional and which not, is arguably essential for spike sorting. Just as with tetrodes, signals from single units are typically present on several nearby channels, and clustering and separation of units is greatly facilitated by taking the whole of the spike waveform into account (Gray et al., 1995; Harris et al., 2000; Blanche et al., 2005; Buzsaki 2004; Swindale and Spacek, 2014; Kadir et al., 2014; Rossant et al., 2015). Event detection, which requires that simultaneous, or near-simultaneous, threshold-crossing signals on different channels be recognized as possibly coming from the same unit is also a step that is critically dependent on a knowledge of channel positions (Jäckel et al., 2012; Rossant et al., 2015; Swindale and Spacek, 2015). Localizing the unit in space relative to the electrode sites is often an important measurement and also requires knowledge of functioning channels and their location. Current Source Density (CSD) analysis (Mitzdorf, 1985), which is often performed on local field potentials recorded with electrode arrays, is also highly susceptible to errors in electrode function and location since it relies on the second spatial derivative of signals. This paper has presented a simple method for detecting non-functional and

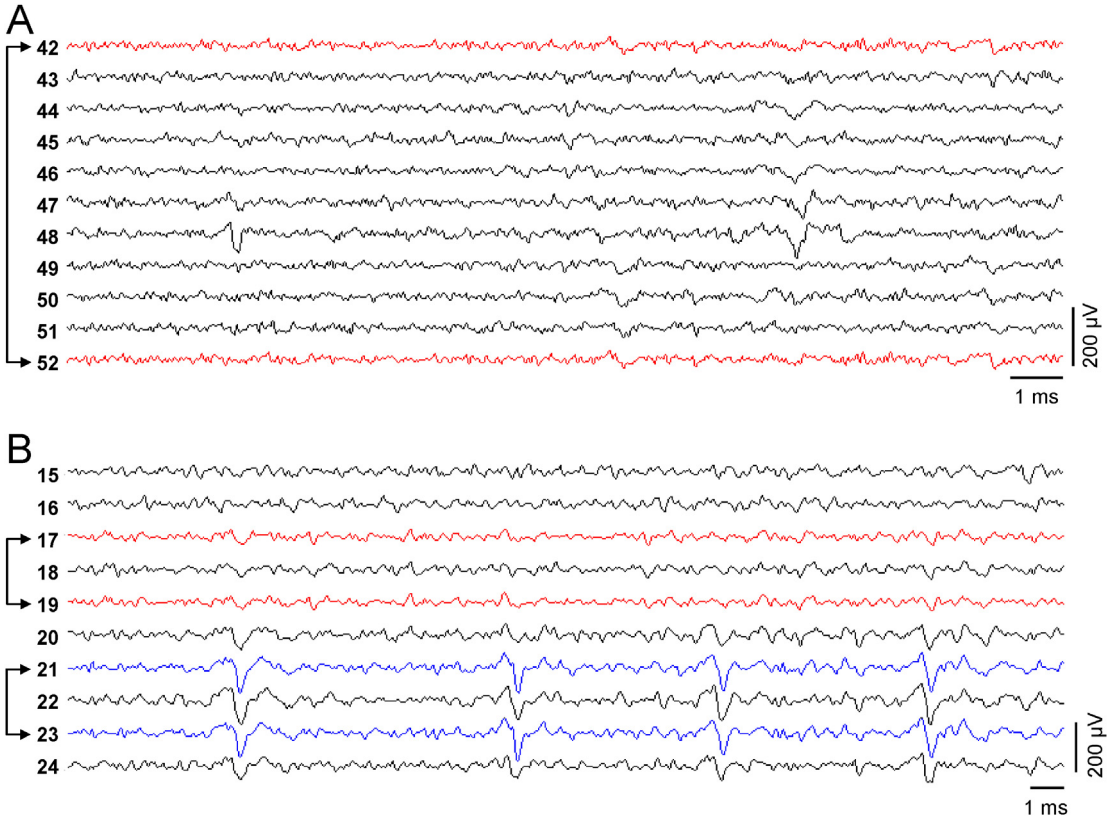

Fig. 4. Raw voltage traces from subsets of channels in datasets R4 (A) and R5 (B). Channel numbers are shown on the left hand side. Channel pairs connected by arrows show highly correlated signals and were identified as outliers by the analysis. Traces are colored to facilitate comparison.

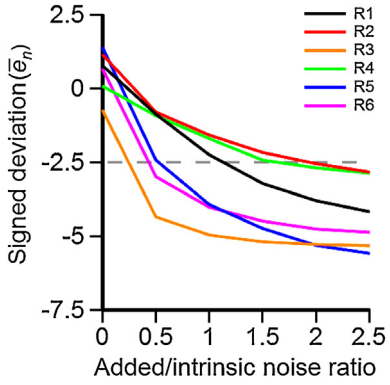

Fig. 5. Values of the signed deviation, $\bar{e}_n$, as a function of the amplitude of a spurious Gaussian noise signal added to a single channel (channel $n = 1$) for the six different datasets R1–R6. Values on the *x*-axis show the ratio of the standard deviation of added Gaussian noise to the standard deviation of the intrinsic voltage signal on the channel. The horizontal dashed line shows the threshold of −2.5 used to classify a measurement as abnormal.

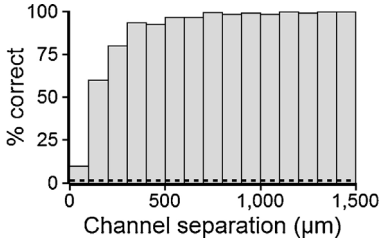

Fig. 6. Histogram showing the percentage of correctly identified location-swapped channels (vertical axis) as a function of the distance between the channels (horizontal axis). Channels were identified as being swapped if the deviation $\bar{d}_n$ for that channel ≥2.5. The false positive rate, *i.e.* the % of channels wrongly identified as mislocalised in the absence of a swap, was 1.3% (dashed line). The analysis is based on swaps of 7,296 channel pairs less than 1500 µm apart.

potentially mislocalised channels that can be applied as a quick screening tool prior to event detection and spike sorting. It is capable of revealing (*a*) channels that have low amplitude or spurious signals unrelated to those on the majority of other channels, perhaps caused by grounding, faulty sites or accidentally disconnected leads; (*b*) shorted channels, and (*c*) mislocalised (or wrongly numbered) channels. In our experience these problems are not infrequent and they are likely to be harder to deal with as channel counts increase, making channel-by-channel inspection tedious and time-consuming. The problems will be briefly discussed in order as follows.

4.1. Faulty or grounded channels

The identities of grounded channels will usually be known if channels have been intentionally grounded on the basis of prior impedance measures. However it may still be useful to check *post-hoc* that the identities were correctly recorded and implemented. Faulty channels (perhaps open circuit or with a physically poor connection) may have large amplitude and/or noisy signals and the identity of these may not always be known in advance. Identification and masking of noisy channels may help in reducing false positives in event detection which would later have to be identified and removed. Although grounded channels are unlikely to produce spurious events, including such channels among those used to estimate the spatial location of a unit (typically done by finding the spatial centre of the distribution of signals across channels) will lead to localization error. Masking non-functional channels will

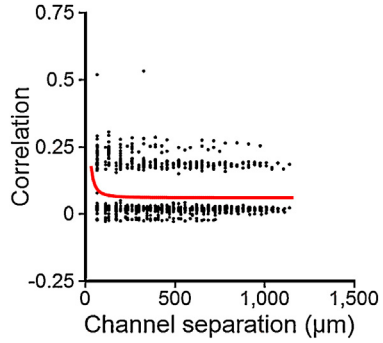

Fig. 7. Correlation-distance plot for a 54 channel electrode (the same electrode used in recording R2) placed in a beaker of saline.

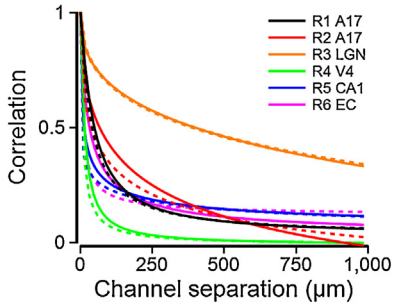

Fig. 8. Comparison of correlation-distance functions found in normal recordings (solid lines) and those found when large amplitude spike signals were masked (dashed lines) as described in the text. The rate of decay was unaltered in one case (recording R3, from the LGN) but was slightly faster in the other recordings. EC—entorhinal cortex.

also remove noise that might interfere with the detection of clusters in principal components or other measures.

4.2. Shorted channels

Detecting shorted channels can be especially tricky as similarity between two waveforms can be hard to spot visually and there will normally be many pairs that might be compared. Deciding what to do with shorted channel pairs in a recording may be difficult. If the two channels are close together the best solution may be to mask one of them and assign the other a position which is the average of the two. If the channels are far apart it may be best to mask both of them rather than deal with signals whose spatial origin is ambiguous. Crosstalk between channels (Figs. 2 and 7) may be the result of physical proximity and parallel trajectory of leads in amplifiers and electronic circuitry. Although the relatively low levels of correlation resulting from this are perhaps unlikely to complicate subsequent spike sorting, such artefactual sources of correlation will need to be taken into account when trying to further characterize the possible biological sources of correlation. Note that given the complexity of arranging leads on MEAs, recording sites that are far apart may be as likely to have leads that are adjacent as channels that are neighbours. Crosstalk may be a factor that contributes to a high baseline (distance independent) level of correlation (parameter C_0, Eq. (1)).

4.3. Mislocalised channels

Correctly matching a channel number in a data file to a physical position on the electrode can be tricky as the relation between a channel's number and its position can be close to arbitrary. The task may be further complicated by the use of patch boxes, inconsistent application of 0-based and 1-based numbering schemes and renumbering imposed by software. If a channel is mislocalised, it is likely that spikes whose waveform is present on both it and another channel will be wrongly detected as two events rather than a single event following event detection. Hence a single unit may be wrongly identified as two different, spatially distinct, units with a spurious high firing correlation. In addition, signals from the mislocalised channel may not be taken into account in assessing spike shape and clustering may be less effective as a result. Attempts to estimate the spatial position of the unit will also suffer.

While the method can identify these problems, it yields suggestive, rather than definitive results (with the exception perhaps of shorted channels) and needs to be followed up by more detailed checks. Because it detects deviations from an overall trend (the decline in correlation with distance) it is also best suited to detecting small numbers of errors. It is unlikely that much specific information will be returned if many channels are mislabelled or mislocalised since this will tend to destroy the orderly relation between channel separation and correlation that the method relies on. However the absence of an obviously orderly relationship might itself suggest the presence of many errors. The method is also not well suited to detecting problems, other than shorted channels, in arrays with spacings >100 μm, where cross-channel correlations would be expected to be low and not to vary much with spacing. A further drawback is that the method is designed to be used in biological recordings, prior to sorting, when it may be too late to correct certain errors. However some problems, such as shorted channels, can be detected in saline recordings (Fig. 7) and it might be worthwhile to carry out such tests prior to using an electrode for recording. We have not tested the method in recordings from *in vitro* cultures or slices, but given that signals in these preparations are also likely to be spatially localised, the method might work provided electrode sites were close enough to detect a range of signal correlation values. As the method relies on the presence of a systematic and consistent decline in correlation with distance it may work less well in situations where there is considerable spatial anisotropy in the decline (*e.g.* due to layer-specific or tangential *vs.* columnar variations) or in situations where combined recordings are being done in different areas (*e.g.* cortex and hippocampus) with substantially different correlation-distance functions. It may be noted that datasets R5 and R6 were simultaneously recorded in CA1 and entorhinal cortex (Table 1) and had similar correlation-distance functions (Fig. 8). When these two recordings were combined, the analysis identified the same 5 abnormal channels shown in Fig. 3C.

The method makes use of the existence of correlations in extracellular voltages that extend over quite long distances in the brain, in some cases up to 500 μm. Because the main goal of the present paper is to make use of these correlations as a means of testing MEA integrity, a more detailed analysis and modelling of the correlations was not attempted. Nevertheless it is of interest to consider some of the possible sources of a correlated signal. While an obvious source of spatially extended signals is spikes, as argued above, the majority of voltage samples on which the correlations were based are likely not to have come from large amplitude (*i.e.* conventionally detectable) spikes but from periods in between. These would normally be considered to represent a 'noise' background on which spikes are superimposed. It is possible that the 'noise' simply consists of many more smaller amplitude spikes, perhaps from larger numbers of neurons a greater distance away. This is perhaps the most likely explanation but it remains to be shown that unresolved neuronal spikes do in fact constitute the main source of low voltage noise in electrophysiological recordings. Another source of correlated voltages could result from LFP signals, which for lower frequencies can extend over long distances (Lindén et al., 2011). The recordings we analyzed however had all been filtered to remove frequencies lower than 500 Hz. Signals above this range would not normally be considered to be part of the LFP, and synaptic potentials, which are believed to constitute a large fraction of the LFP

(Buzsáki et al., 2012) are likewise too slow to contribute to frequencies above 500 Hz. Other sources might be dendritic spikes, which for apical dendrites oriented roughly parallel to the electrode (as in the cortical recordings examined here) could extend over distances of several hundreds of microns.

M.A.S. and N.V.S. jointly performed the experiments from which datasets R1 and R2 are derived; N.V.S. developed the methods, did the analyses and wrote the paper; M.A.S. read and made revisions to the paper.

Acknowledgements

We thank Curtis Baker, Youping Xiao and Artak Khachatryan for contributing data used in this study. We thank Kenji Mizuseki for his help in identifying the channel layout in the R5 and R6 datasets and Curtis Baker for helpful comments on the manuscript. The work was supported by grant MOP 15360 from the Canadian Institutes of Health Research.

References

Berényi A, Somogyvári A, Nagy AJ, Roux L, Long JD, Fujisawa S, et al. Large-scale, high-density (up to 512 channels) recording of local circuits in behaving animals. J Neurophysiol 2014;111:1132–49.

Blanche TJ, Spacek MA, Hetke JF, Swindale NV. Polytrodes high density silicon electrode arrays for large scale multiunit recording. J Neurophysiol 2005;93:2987–3000.

Buzsáki G. Large-scale recording of neuronal ensembles. Nat Neurosci 2004;7:446–51.

Buzsáki G, Anastassiou CA, Koch C. The origin of extracellular fields and currents–EEG, ECoG, LFP and spikes. Nat Rev Neurosci 2012;13:407–20.

Drake KL, Wise KD, Farraye J, Anderson DJ, BeMent SL. Performance of planar multisite microprobes in recording extracellular single-unit intracortical activity. IEEE Trans Biomed Eng 1988;35:719–32.

Gray CM, Meldonado PE, Wilson M, McNaughton B. Tetrodes markedly improve the reliability and yield of multiple single-unit isolation from multi-unit recordings in cat striate cortex. J Neurosci Methods 1995;63:43–54.

Harris KD, Henze DA, Csicsvari J, Hirase H, Buzsáki G. Accuracy of tetrode spike separation as determined by simultaneous intracellular and extracellular measurements. J Neurophysiol 2000;84:401–14.

Jäckel D, Frey U, Fiscella M, Franke F, Hierlemann A. Applicability of independent component analysis on high-density microelectrode array recordings. J Neurophysiol 2012;108:334–48.

Kadir SN, Goodman DFM, Harris KD. High-dimensional cluster analysis with the masked EM algorithm. Neural Comput 2014;26:2379–94.

Lindén H, Tetzlaff T, Potjans TC, Pettersen KH, Grün S, Diesmann M, et al. Modeling the spatial reach of the LFP. Neuron 2011;72(5):859–72.

Mitzdorf U. Current source-density method and application in cat cerebral cortex: investigation of evoked potentials and EEG phenomena. Physiol Rev 1985;65:37–100.

Press WH, Teukolsky SA, Vetterling WT, Flannery BP. Numerical recipes. The art of scientific computing. 2nd ed. Cambridge, MA: Cambridge University Press; 1994.

Rossant C, Kadir SN, Goodman DF, Schulman J, Belluscio M, Buzsaki G, et al. Spike sorting for large, dense electrode arrays; 2015. p. 015198, bioRxiv.

Swindale NV, Spacek MA. Spike sorting for polytrodes: a divide and conquer approach. Front Syst Neurosci 2014;8(6):1–21, http://dx.doi.org/10.3389/fnsys.2014.00006.

Swindale NV, Spacek MA. Spike detection methods for polytrodes and high density microelectrode arrays. J Comput Neurosci 2015;38:249–61, http://dx.doi.org/10.1007/s10827-014-0539-z.